Large and Recoverable Electrostrain in Strained Ferroelectric Superlattices due to Domain Switching

JIANG Zhexin[1,2], *WANG Jie*[1,2*]

1. School of Aeronautics and Astronautics, Zhejiang University, Hangzhou 310027, P. R. China;
2. Key Laboratory of Soft Machines and Smart Devices of Zhejiang Province, Zhejiang University, Hangzhou 310027, P. R. China

(Received 30 November 2020; revised 21 January 2021; accepted 1 February 2021)

Abstract: The ferroelectric superlattices have been widely studied due to their distinguished electromechanical coupling properties. Under different biaxial mismatch strains, ferroelectric superlattices exhibit different domain structures and electromechanical coupling properties. A three-dimensional phase field model is employed to investigate the detailed domain evolution and electromechanical properties of the $PbTiO_3/SrTiO_3$ (PTO/STO) superlattices with different biaxial mismatch strains. The phase field simulations show that the ferroelectric superlattice exhibits large electrostrain in the stacking direction when an external field is applied. Under a large compressive mismatch strain, vortex domains appear in ferroelectric layers with the thickness of 4 nm. The vortex domains become stable c-domain under a large external electric field, which remains when the electric field is removed. When the initial compressive mismatch strain decreases gradually, the waved or a1/a2 domains replaces the initial vortex domains in the absence of electric field. The fully polarized c-domain by a large electric field switches to diagonal direction domain or a/c domain when the electric field is small. Furthermore, when a biaxial tensile strain is applied to the superlattice, ferroelectric domains switch back to the initial a1/a2 twin-like domain structure, resulting in the recoverable and large electrostrain. This provides an effective way to obtain the large and recoverable electrostrain for the engineering application.

Key words: large electrostrain; ferroelectric superlattices; domain switching; recoverable domains

CLC number: TB381 **Document code:** A **Article ID:** 1005-1120(2021)01-0075-09

0 Introduction

Ferroelectric materials have been widely used in many electronic and electromechanical devices such as memories and actuators due to their unique dielectric, ferroelectric and piezoelectric properties. The properties of ferroelectric materials are closely related to the polarization distribution and domain structures. Below the Curie temperature, ferroelectric materials with different compositions usually possess various kinds of domain structures. These domain structures are often dependent not only on the compositions but also on the geometries. Due to the dependence of domain structures on compositions and geometries, different structures[1] and compositions[2-3] have been designed to tune the domain structures and the electromechanical coupling properties of ferroelectric materials. Meanwhile, the influence of temperature[4], stress[5] and electric field[6-7] on the electromechanical coupling properties of ferroelectric materials have also been studied by many researchers. Due to the controllability of electric field, controlling domain switching by external electric field to achieve the optimal performance has attracted much attention.

In addition to ferroelectric single crystals and ceramics, the interesting properties of ferroelectric superlattices have gradually become a research hot-

*Corresponding author, E-mail address: jw@zju.edu.cn.

How to cite this article: JIANG Zhexin, WANG Jie. Large and recoverable electrostrain in strained ferroelectric superlattices due to domain switching[J]. Transactions of Nanjing University of Aeronautics and Astronautics, 2021, 38(1): 75-83.
http://dx.doi.org/10.16356/j.1005-1120.2021.01.007

spot in recent years[8]. The improvement of experimental techniques about epitaxial strain and layer-by-layer growth led scientists to produce high quality nanometer ferroelectric superlattices. For example, Yadav et al. used pulsed-laser deposition method to synthesize ferroelectric superlattice films with different period-thicknesses[9]. Due to the different thicknesses of ferroelectric and dielectric layers in superlattices, domain structures are known to include a1/a2 domain, a/c domain, flux-closure domain, vortex domain[10] and polar skyrmions[11]. Hong et al. predicted that vortex structures appear in the superlattice grown on the $DyScO_3$ substrate when the thickness of the ferroelectric layer is 4 nm. If the external fields such as stress, strain and electric field are considered, more domains with special morphologies could be generated and mixed.

In this work, the influence of the biaxial misfit strain on the domain structures and electromechanical response of the three-dimensional ferroelectric superlattice ($PbTiO_3$(PTO)/$SrTiO_3$(STO)) is investigated by using the phase field model. In order to get the domain evolution and electromechanical response, a quasi-static cyclic electric field is applied in the stacking direction of the ferroelectric superlattice. The large range of electrostrain induced by the switching of domain structure and the change of polarization magnitude is the focus of the work. The recoverable and large electrostrain due to the domain switching from a1/a2 domain to c-domain under a biaxial tension strain is predicted.

1 Phase Field Modeling

In order to study the polarization evolution in ferroelectric superlattices, phase field method is frequently used. Phase field method has great advantage in investigating the influence of electric field and stress/strain on the evolution of ferroelectric domain structure. It can not only qualitatively reveal the detailed shapes of domain and domain wall, but also quantitatively calculate the polarization and electric field. In this study, the polarization vector $\boldsymbol{P}=(P_1,P_2,P_3)$ is chosen as the order parameter, and the polarization spatial distribution represents ferroelectric domain structure. Various properties of superlattice can be derived from domain structure. The temporal evolution of the domain structure can be obtained by solving the time-dependent Ginzburg-Landau (TDGL) equations[12]

$$\frac{\partial P_i(\boldsymbol{r},t)}{\partial t}=-L\frac{\delta F}{\delta P_i(\boldsymbol{r},t)} \qquad i=1,2,3 \tag{1}$$

where L, $\boldsymbol{r}$ and t denote the kinetic coefficient, spatial position vectors and time, respectively.

The total free energy of ferroelectric materials ($F=\int_V f\,\mathrm{d}V$) includes the Landau free energy, the domain wall energy, the elastic energy and the electric energy. For the PTO and STO in the superlattice, their energy forms can be expressed as the following functions related to polarization P_i, strain ε_{ij} and electric field E_i, shown as

$$\begin{aligned}F=\int[&\alpha_i P_i^2+\alpha_{ij}P_i^2P_j^2+\alpha_{ijk}P_i^2P_j^2P_k^2+\\&\frac{1}{2}g_{ijkl}\left(\frac{\partial P_i}{\partial x_j}\frac{\partial P_k}{\partial x_l}\right)+\frac{1}{2}c_{ijkl}\varepsilon_{ij}\varepsilon_{kl}-q_{ijkl}\varepsilon_{ij}P_kP_l-\\&\frac{1}{2}\varepsilon_0\varepsilon_r E_iE_i-E_iP_i]\,\mathrm{d}V\end{aligned} \tag{2}$$

where α_i, α_{ij}, α_{ijk} are the Landau energy coefficients; g_{ijkl} is the gradient energy coefficient, c_{ijkl} the elastic constant, and q_{ijkl} the electrostrictive coefficient; ε_0 and ε_r represent the dielectric constant of the vacuum and relative dielectric constant of the background material ($\varepsilon_r=66$ for PTO and $\varepsilon_r=300$ for STO), respectively.

In addition, both the mechanical equilibrium equations

$$\sigma_{ij,j}=\frac{\partial}{\partial x_j}\left(\frac{\partial f}{\partial \varepsilon_{ij}}\right)=0 \tag{3}$$

and the Maxwell's equations

$$D_{i,i}=-\frac{\partial}{\partial x_i}\left(\frac{\partial f}{\partial E_i}\right)=0 \tag{4}$$

should be satisfied at the same time, where σ_{ij} is the stress displacement component, D_i the electric displacement component and f the free-energy density.

Following previous work[12], the spontaneous strains are related to spontaneous polarizations, which are given by[13]

$$\begin{cases}\varepsilon_{11}^0 = Q_{11}P_1^2 + Q_{12}(P_2^2 + P_3^2)\\ \varepsilon_{22}^0 = Q_{11}P_2^2 + Q_{12}(P_1^2 + P_3^2)\\ \varepsilon_{33}^0 = Q_{11}P_3^2 + Q_{12}(P_1^2 + P_2^2)\\ \varepsilon_{23}^0 = Q_{44}P_2P_3\\ \varepsilon_{13}^0 = Q_{44}P_1P_3\\ \varepsilon_{12}^0 = Q_{44}P_1P_2\end{cases} \quad (5)$$

where Q_{ij} are the electrostrictive coefficients.

In this work, the semi-implicit Fourier-spectral method is employed to numerically solve the related equations[14]. All of the related material parameters of PTO and STO at room temperature are taken from previous works[15]. Table 1 lists all the related material parameters of PTO and STO with SI units, and the unit of temperature T is K. Small random fluctuation ($<0.01P_0$, where $P_0 = 0.757\ \mathrm{C/m^2}$ is the spontaneous polarization of PTO at room temperature) is used as the initial values to initiate the domain evolution.

Table 1 Material parameters of PTO and STO

Parameter	PTO	STO
$\alpha_1/(10^5\mathrm{C^{-2}\cdot m^2\cdot N})$	$3.8(T-752)$	$7.06(T-35.5)$
$\alpha_{11}/(10^8\mathrm{C^{-4}\cdot m^6\cdot N})$	−0.73	17.00
$\alpha_{12}/(10^8\mathrm{C^{-4}\cdot m^6\cdot N})$	7.5	13.7
$\alpha_{111}/(10^8\mathrm{C^{-6}\cdot m^{10}\cdot N})$	2.6	0.0
$\alpha_{112}/(10^8\mathrm{C^{-6}\cdot m^{10}\cdot N})$	6.1	0.0
$\alpha_{123}/(10^8\mathrm{C^{-6}\cdot m^{10}\cdot N})$	−37	0
$Q_{11}/(\mathrm{C^{-2}\cdot m^4})$	0.089 0	0.045 7
$Q_{12}/(\mathrm{C^{-2}\cdot m^4})$	−0.026 0	−0.013 5
$Q_{44}/(\mathrm{C^{-2}\cdot m^4})$	0.067 50	0.009 57
$C_{11}/(10^{11}\mathrm{m^{-2}\cdot N})$	1.746	3.156
$C_{12}/(10^{11}\mathrm{m^{-2}\cdot N})$	0.79	1.01
$C_{44}/(10^{11}\mathrm{m^{-2}\cdot N})$	1.11	1.19
$g_{11}/(10^{-11}\mathrm{C^{-2}\cdot m^4\cdot N})$	3.46	3.46
$g_{12}/(10^{-11}\mathrm{C^{-2}\cdot m^4\cdot N})$	0	0
$g_{44}/(10^{-11}\mathrm{C^{-2}\cdot m^4\cdot N})$	1.73	1.73

Fig.1 shows the three-dimensional model of ferroelectric superlattices. The x, y and z axes are parallel to the [1 0 0], [0 1 0] and [0 0 1] crystallographic directions, respectively. The structure consists of six layers, including three layers of ferroelectric film (PTO) and three layers of dielectric film (STO). Monolayer of PTO and STO are stacked alternately along the z-axis direction. In order to generate vortex domain in the ferroelectric layer, the thickness of each layer is set to be 4 nm. Periodic boundary conditions are used in the stacking direction and in-plane direction. A three-dimensional mesh of 100 × 100 × 60 is used. Each grid is set as 0.4 nm to simulate the lattice size of the material approximately. The four arrows in Fig.1 represent uniformly distributed biaxial strains (ε_{xx} and ε_{yy}) in the x and y directions. A vertical quasi-static electric field is applied in the z direction. Here, to meet the periodic boundary conditions in the stacking direction, uniform electric field is applied instead of the electric potential.

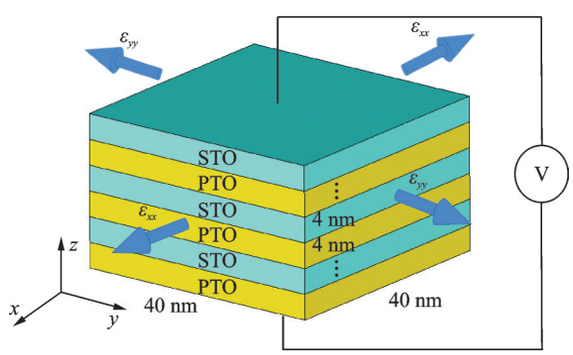

Fig.1 Schematic diagram of 3-D ferroelectric superlattices under given biaxial strains and vertical electric field

2 Results and Discussion

Under the large biaxial compressive strain of $\varepsilon_{xx} = \varepsilon_{yy} = -1\%$, Fig.2 shows the polarization direction and the polarization component in the z direction denoted by black arrows and color contour, respectively. The panels in Fig.2 are the domain states in the whole simulated model, while the below panels are the detailed polarization distribution in the white squares of the panels. The colors in Fig.2 denote the magnitudes of polarization components in the z direction. It can be seen that the stripe vortex domain structure in the ferroelectric layer in Fig.2(a) is a stable initial state under large biaxial compression strain when the layer thickness is set as 4 nm. Under a large compression strain, vortex and anti-vortex domains appear in the ferroelectric and dielectric layers of superlattice due to the competition among electric field energy, strain energy and domain wall energy[8-9]. When the vertical electric field increases, the vortex domain structures are destroyed gradually. When superlattice finally reaches

the state of single domain, the domain structure in superlattice is transformed into single c-domain and has the same polarization direction in the ferroelectric and the dielectric layer, as shown in Fig.2(b). As a major characteristic of ferroelectric materials, residual polarization also exists in ferroelectric superlattices. When the external electric field is removed, the domain structure in the superlattice remains, but the polarization magnitude decreases significantly. Because the in-plane domains are unfavorite under the large compressive strain, the out-of-plane polarization is induced by the vertical electric field, which are shown by the color contour in Fig.2(b) and Fig.2(c).

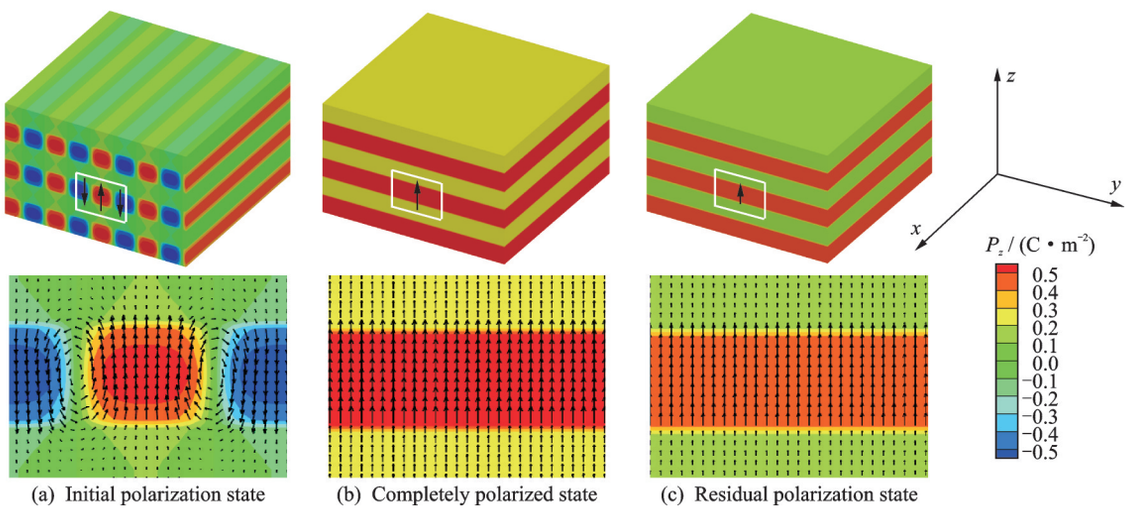

Fig.2 Polarization distributions of the superlattice with different states

Based on the polarization along the stacking direction in the ferroelectric and dielectric layers, the average polarization of the whole superlattice is calculated. The hysteresis loop curves under different biaxial strains are plotted in Fig.3, in which the numbers 1, 2, 3 and their nearest solid lines represent the three domains in Figs.3(d—f), respectively. The blue lines and numbers represent the transition of the electric field from positive to negative, while the red ones represent the opposite. The arrows of solid line represent the order in which the polarization and domain structure change in a cyclic electric field.

The domain structures in Fig.2(b) and Fig.2(c) correspond to the two points where the electric field are equal to 60 and 0 kV/mm, respectively, in the hysteresis loop of Fig.3(a). Under large compressive stain, the c-domain remains up or down in the vertical direction. Even if the electric field is removed, the initial vortex state cannot be recovered. However, when the strain decreases, the situation begins to change. Fig.3(b) shows that when the biaxial strain is −0.5%, the shape of hysteresis loop begins to change, and the numbers of domain types begin to increase. When the positive electric field turns to the opposite direction, the c-domain in ferroelectric layer becomes unstable. Without the restrain of large biaxial compressive strain, the domain structure begins to switch to the in-plane direction, thus the diagonal direction domain and a/c domain appear. Moreover, with the further decrease of the compressive strain, the range of electric field generating the c-domain further shrinks, and the electric field required for generating the single domain is larger. When the electric field is small, the a/c domain and the diagonal direction domain become the dominant domain structure in the superlattice.

It should be noted that during the quasi-static loading and unloading of electric field, the variation of domain structure is not the same. The hysteresis loop is symmetric with respect to the center. With the decrease of biaxial misfit compression strain, the enclosed area of the hysteresis loop gradually shrinks. This suggests that it is possible to close the hysteresis loop by adjusting the biaxial misfit strain.

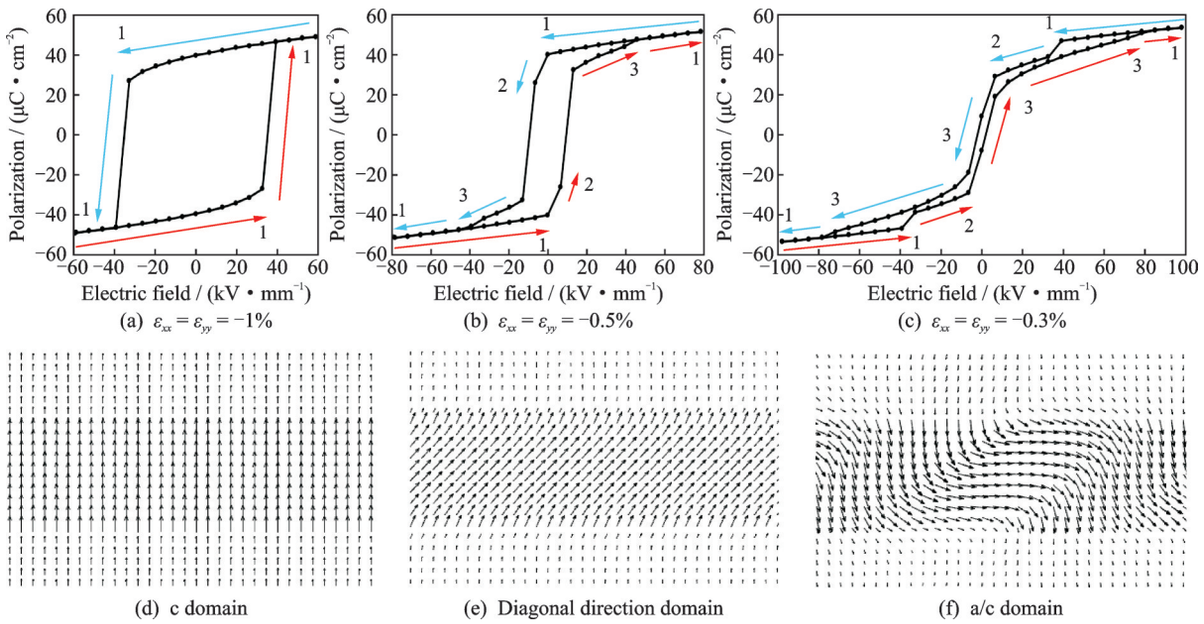

Fig.3 Hysteresis loops and typical domain structures of the superlattice under different biaxial compression strains

The closing of the hysteresis loop means that the coercive field is eliminated, so the recoverable electrostrain is possible.

According to spontaneous strain equations of Eq.(5), the electrostrain of the superlattice can be obtained by the average polarization and the related electrostrictive coefficient. Under three different biaxial compression strains, the curves of electrostrain versus electric field are presented in Fig.4. Lines and numbers in Fig.3 and Fig.4 correspond one to one. The strain calculated refers to the electrostrain along the stacking direction of the superlattice. Fig.4(a) is a common butterfly-shaped loop of ferroelectric strain versus electric field. Due to the change of domain structure, the corresponding loop of strain versus electric field deforms, as shown in Fig.4(b) and Fig.4(c). For the biaxial misfit strains of -1%, -0.5% and 0.3%, the electric fields for inducing single domain are 40, 50 and 80 kV/mm, respectively. Although the magnitudes of the electric field leading to the single domain are not the same, the electrostrains induced by the same electric field are basically equal in the saturated states for the three cases. Therefore, to find the largest change of electrostrain within a limited range of electric field, we focus on the lowest point of the electrostrain curve rather than the highest point. By comparing the three curves in Fig.4, the decline of the lowest points is obvious. Although the decrease of the biaxial compression strain leads to the increase of the saturated electric fields, the largest variation of electrostrain increases. The largest variation of electrostrain mainly results from the domain switching from out-of-plane to the in-plane direction. When c-domain has only the 180° switching, the magnitude of polarization component P_z along

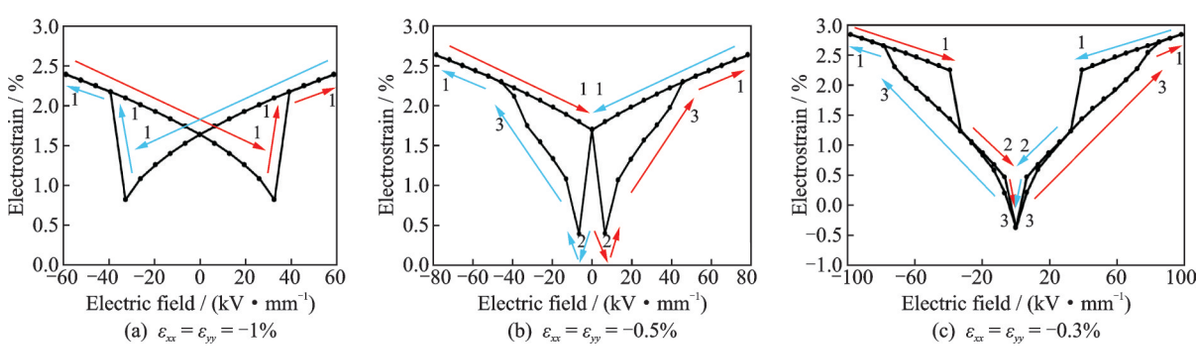

Fig.4 Electrostrain curves of the superlattice under different biaxial compression strains

the stacking direction is still relatively large. However, when c-domain turns into diagonal direction domain or a/c domain, P_z decreases significantly, which causes the lowest point of electrostrain curves to go down. Under the biaxial compression strain of -0.3%, considering the state just reaches the single domain, the superlattice has the electrostrain range of over 3%, which is more than twice as much as that of -1%.

It has been shown that the decreases of biaxial compressive strain increase the variation of electrostrain. However, the vortex or waved domain structures in the initial state do not have good recoverability under a small compressive strain. When the electric field is removed, the ferroelectric layer of the superlattice is more inclined to form a/c domain to minimize the total energy, which causes the electrostrain in the stacking direction fail to return back to its original state. In order to solve this problem, a regulated way of applying tensile strain is considered. It is found that in the initial state, a1/a2 domain is stable in the superlattices under biaxial misfit tensile strain. Similar domain structures have been reported in the work of Hong et al.[10], but the a1/a2 domain is realized by limiting the thickness of ferroelectric layers. In our simulation, a1/a2 domain structure can be realized under larger thickness size by applying the tensile misfit strain. More surprisingly, the domain structure is recoverable under the biaxial tensile strain. As shown in Fig. 5(a), when the external electric field is removed, the domain structure of the superlattice will eventually switch back to the a1/a2 domain, and the color contour indicates the size and direction of P_x. Figs.5(b—d) represent the detailed polarization distribution of the corresponding area in the white box. It must be stated that for the initial state, the direction of a1/a2 domain is same at the same position in each layer, but the domain structure recovered from c-domain is not. As can be clearly seen from Fig.5, the a1/a2 domains in the adjacent ferroelectric layers are in opposite directions, while the domains in the ferroelectric layers separated by one layer are in the same direction. Due to the polarization along the stacking direction of a1/a2 domain is almost negligible and the contribution of in-plane polarization to electrostrain in the stacking direction is the same, the differences in domain directions have no influence and the recoverability of electrostrain is obtained.

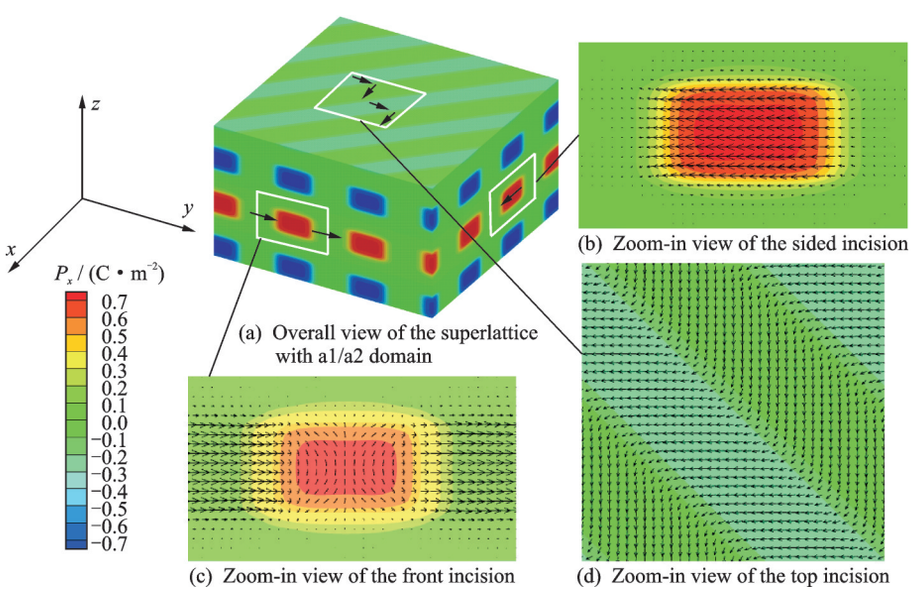

Fig.5 Simulated a1/a2 domain in the superlattice and polarization distributions of its three incisions

Using the same method as Fig.3 and Fig.4, we plot curves of the polarization versus electric field and the electrostrain versus electric field under two biaxial misfit tensile strains in Fig.6. The tensile strains of 0.3% and 0.5% correspond to Figs.6(a, b), respectively. The solid lines, colors, and num-

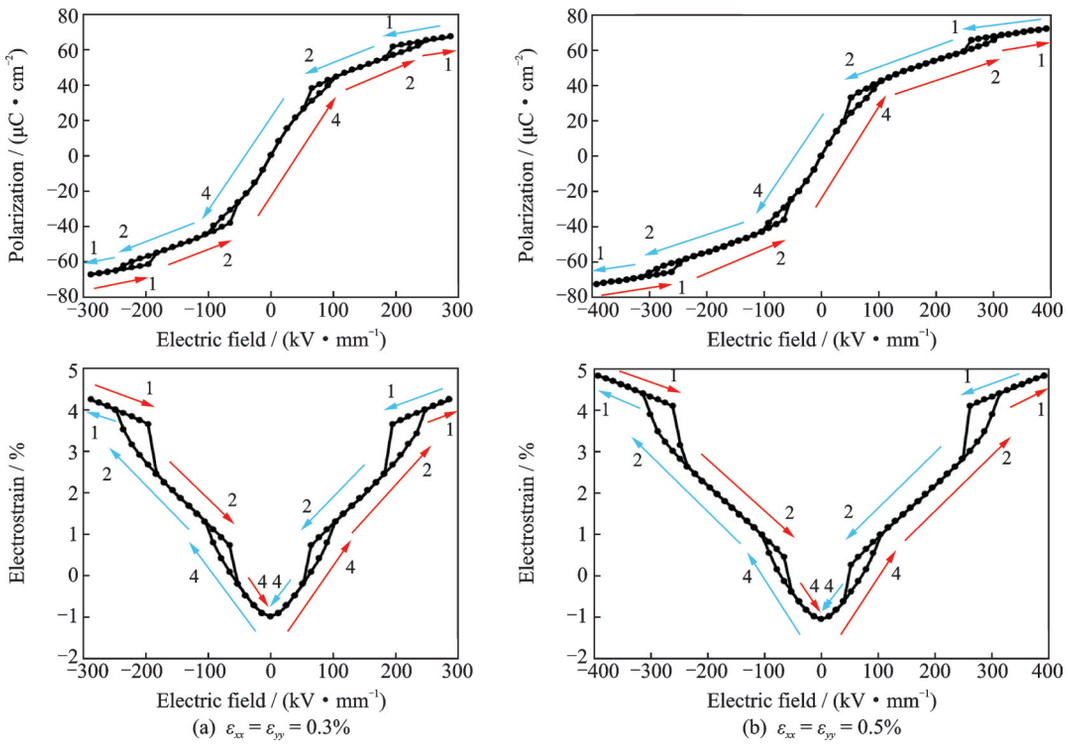

Fig.6 Polarization versus electric field and electrostrain versus electric field under different tensile misfit strains

bers have the same meaning as in Figs.3, 4, excepting that the new number 4 represents the a1/a2 domain. It is clear that a/c domain has been replaced by a1/a2 domain under the biaxial tensile strain. This change is responsible for the recoverability of the electrostrain. It can be seen from Fig.6(a) that when the electric field is fully removed, the average polarization in the stacking direction returns to zero, which also means the absence of coercive fields. When the electric field changes from −50 kV/mm to 50 kV/mm, electrostrain curve has no hysteresis loop. When the electric field extends the range from −50 kV/mm to 50 kV/mm, two small hysteresis loops appear in the curve, which is caused by the different evolution of domain structures during the loading and unloading of electric field. Since what we seek is the largest range between the maximum and minimum electrostrain induced by electric field and the ability of turning back to the initial deformation state after the electric field is removed, the models and outcomes are all acceptable.

As mentioned above, the smaller the compressive strain is, the lower the value of the minimum electrostrain will be. However, by comparing the influence of different biaxial tensile strains on electrostrain in Figs.6(a,b), we find the above effect is almost negligible, because the contribution of a1/a2 domain to P_z is already very small. The further increase of biaxial tensile misfit strain has little influence on the lowest point of electrostrain. Therefore, a small biaxial tensile misfit strain is enough for the superlattice to achieve the largest electrostrain range. When the single domain is formed, the polarization and electrostrain are always equal under the same electric field, no matter tensile strain or compressive strain. For the superlattice with the biaxial strain of 0.3%, an electric field of 250 kV/mm is required to achieve the single domain state. Based on the domain switching from initial a1/a2 domain to single c-domain, 5% electrostrain along the stacking direction is obtained.

3 Conclusions

In summary, the influence of biaxial misfit strains on the evolution of domain structures in the PTO/STO superlattices has been studied. The hysteresis loops and electrostrain curves are obtained for the superlattices under different electric fields and misfit strains. The different domain structures and evolution processes are found under different

misfit strains and electric fields. It is found that the 5% electrostrain along the stacking direction is obtained under a small biaxial tensile misfit strain. In addition, when the external electric field is removed, the fully polarized c-domain switches back to the initial a1/a2 domain and the electrostrain in the stacking direction recovers to the initial state. The present work provides an effective way to realize large and recoverable electromechanical response of ferroelectric nanomaterials by using domain engineering and strain engineering.

References

[1] CHEN H, HOU X, CHEN J, et al. Large electrostrain induced by reversible domain switching in ordered ferroelectric nanostructures with optimized geometric configurations[J]. Nanotechnology, 2020, 31(33): 335714.

[2] LI Y L, HU S Y, CHEN L Q. Ferroelectric domain morphologies of (001) $PbZr_{1-x}Ti_xO_3$ epitaxial thin films[J]. Journal of Applied Physics, 2005. DOI: 10.10631/1.1849820.

[3] LI W, LIU X, MA J, et al. Low temperature sintering and properties of lead-free $(Ba_{0.85}Ca_{0.15})(Zr_{0.1}Ti_{0.9})O_3$ ceramics with $Ba(Cu_{0.5}W_{0.5})O_3$ addition[J]. Journal of Materials Science: Materials in Electronics, 2013, 24(5): 1551-1555.

[4] WANG X S, WANG C L, ZHONG W L, et al. Polarization and dielectric properties of temperature-graded ferroelectric structure from the transverse Ising model[J]. Materials Science and Engineering B: Solid-State Materials for Advanced Technology, 2003, 99(1/2/3): 576-579.

[5] PARK S E, SHROUT T R. Ultrahigh strain and piezoelectric behavior in relaxor based ferroelectric single crystals[J]. Journal of Applied Physics, 1997, 82(4): 1804-1811.

[6] QIU Y, WU H, WANG J, et al. The enhanced piezoelectricity in compositionally graded ferroelectric thin films under electric field: A role of flexoelectric effect[J]. Journal of Applied Physics, 2018, 123(8): 084103.1-084103.8.

[7] LI Y L, HU S Y, LIU Z K, et al. Effect of electrical boundary conditions on ferroelectric domain structures in thin films[J]. Applied Physics Letters, 2002, 81(3): 427-429.

[8] DU K, ZHANG M, DAI C, et al. Manipulating topological transformations of polar structures through real-time observation of the dynamic polarization evolution[J]. Nature Communications, 2019, 10(1): 1-8.

[9] YADAV A K, NELSON C T, HSU S L, et al. Observation of polar vortices in oxide superlattices[J]. Nature, 2016, 530(7589): 198-201.

[10] HONG Z, DAMODARAN A R, XUE F, et al. Stability of polar vortex lattice in ferroelectric superlattices[J]. Nano Letters, American Chemical Society, 2017, 17(4): 2246-2252.

[11] DAS S, TANG Y L, HONG Z, et al. Observation of room-temperature polar skyrmions[J]. Nature, 2019, 568(7752): 368-372.

[12] LI Y L, HU S Y, LIU Z K, et al. Effect of substrate constraint on the stability and evolution of ferroelectric domain structures in thin films[J]. Acta Materialia, 2002. DOI: 10.1016/S1359-6454(01)00360-3.

[13] WANG J, SHI S Q, CHEN L Q, et al. Phase-field simulations of ferroelectric/ferroelastic polarization switching[J]. Acta Materialia, 2004, 52(3): 749-764.

[14] CHEN L Q, SHEN J. Applications of semi-implicit Fourier-spectral method to phase field equations[J]. Computer Physics Communications, 1998, 108(2/3): 147-158.

[15] CHEN L. APPENDIX A—Landau free-energy coefficients[J]. Physics of Ferroelectrics, 2007, 372(3): 363-371.

Acknowledgements This work was supported by the National Natural Science Foundation of China (Nos. 11672264, 11972320) and the Zhejiang Provincial Natural Science Foundation (No. LZ17A020001).

Authors Mr. **JIANG Zhexin** received the bachelor of engineering science in engineering mechanics from Zhejiang University, Hangzhou, China, in 2018. Currently, he is studying for master's degree in solid mechanics in Zhejiang University. His research has focused on phase field modeling on the characteristics of ferroelectric superlattice materials, including electrostrain and negative capacitance.

Prof. **WANG Jie** received his bachelor degree from Xi'an Jiaotong University in 1998, master degree from Lanzhou University in 2002, and Ph.D. degree from the Hong Kong University of Science and Technology (HKUST) in 2006. He worked as a postdoctoral research associate at HKUST (2006—2007) and as a Humboldt research fellow at Karlsruhe Institute of Technology in Germany (2007—2009). He joined Zhejiang University as an associate professor in 2009 and was promoted as a full professor in 2015. From 2012 to 2014, he has been visiting Kyoto University as a JSPS research fellow. His research mainly focuses on the first-princi-

ple calculations and phase field modeling on the multi-field coupling properties of ferroelectric, ferromagnetic and multiferroic materials.

Author contributions Mr. **JIANG Zhexin** designed the study, built the models, conducted the analysis, interpreted the results and wrote the manuscript under the supervision of Prof. **WANG Jie**. All authors commented on the manuscript draft and approved the submission.

Competing interests The authors declare no competing interests.

(Production Editor: ZHANG Huangqun)

铁电超晶格中畴变导致的可恢复大电致应变

蒋哲鑫[1,2], 王 杰[1,2]

(1.浙江大学航空航天学院,杭州 310027,中国;
2.浙江大学浙江省软体机器人与智能器件研究重点实验室,杭州 310027,中国)

摘要:铁电超晶格由于其独特的机电耦合特性而得到了广泛的研究。在不同的双轴错配应变下,铁电超晶格表现出不同的畴结构和机电耦合特性。本文采用三维相场模型研究了不同双轴错配应变下$PbTiO_3$/$SrTiO_3$(PTO/STO)超晶格的畴演化和机电性能。相场模拟结果表明,外加电场作用下铁电超晶格在堆叠方向上表现出较大的电致应变。在较大的错配压应变下,厚度为4 nm的铁电层中会出现涡旋畴。在外加大电场作用下,涡旋畴变为稳定的c畴,去除电场后c畴依旧保持。当错配压应变逐渐减小时,无外电场下的初始涡旋畴会变为波浪畴或a1/a2畴。此时,大电场作用下完全极化后的c畴在电场变小后会转变为对角线方向畴或a/c畴。此外,当对超晶格施加双轴拉应变时,铁电畴能够翻转回初始的a1/a2类孪晶畴结构,从而产生可恢复的大电致应变。本文研究提供了获得可恢复大电致应变的有效途径。

关键词:大电致应变;铁电超晶格;畴切换;可恢复畴